value of +37.6 ± 1.2 cm^3 mol^{-1} is not too far away from our value of +26.5 ± 2.4 cm^3 mol^{-1}, demonstrating that the apparent discrepancy in $\Delta\bar{V}(K)$ does not affect the mechanistic interpretation for the electron-transfer step itself. Furthermore, Saito and coworkers[42] also reported a $\Delta\bar{V}(K)$ value of +23 ± 3 cm^3 mol^{-1} for the $Co(NH_3)_5py^{3+}/Fe(CN)_6^{4-}$ system, and the large deviation from the data for the corresponding aquo system (see above) remains uncertain. These discrepancies encourage us to point out that the precursor formation step probably involves more than pure electrostatic interaction, and it is quite possible that solvent molecules may not be released to such an extent as expected for the neutralization of charges accompanied by a decrease in electrostriction. A partial overlap of the molecular orbitals of the reactants may counteract the volume increase due to charge neutralization and result in overall negative $\Delta\bar{V}(K)$ values. The data in Tables II and III seem to support a slight increase in K with increasing viscosity, indicating that the thermodynamic stability of the precursor (ion pair) is affected to some extent by the viscosity of the medium.

We conclude that the results of the present study once again underline the importance of solvent rearrangement and collision processes in controlling the dynamics of the electron-transfer reaction in outer-sphere processes. The results can be understood in a qualitative way by considering the limitations of the transition-state theory and taking the dynamic effect of the reaction medium into account.

Acknowledgment. We gratefully acknowledge financial support from the Max Buchner Forschungsstiftung, the Deutsche Forschungsgemeinschaft, and the Fonds der Chemischen Industrie.

Supplementary Material Available: Listings of k_{obsd} for the reduction of $Co(NH_3)_5H_2O^{3+}$ by $Fe(CN)_6^{4-}$ as a function of temperature and [Fe(II)] (Table A) and as a function of pressure and [Fe(II)] (Table B) (2 pages). Ordering information is given on any current masthead page.

(42) Kanesato, M.; Ebihara, M.; Sasaki, Y.; Saito, K. *J. Am. Chem. Soc.* **1983**, *105*, 5711.

Contribution from the Chemistry Department, University of Houston, University Park, Houston, Texas 77204

Equilibrium of 17-Electron and 19-Electron Organometallic Radicals Derived from Carbonylmanganese Anions and Cations

D. J. Kuchynka and J. K. Kochi*

Received August 26, 1988

The transient 17-electron carbonylmanganese(0) radical $Mn(CO)_5^{\bullet}$ produced from the oxidation of $Mn(CO)_5^-$ is detected with the reversible potential E° = 0.085 V vs SCE by fast-scan cyclic voltammetry using platinum microelectrodes. The persistence of the substituted carbonylmanganese(0) radicals is prolonged by increasing numbers of phosphine ligands (P) in $Mn(CO)_4P^{\bullet}$ and $Mn(CO)_3P_2^{\bullet}$ radicals. In contrast, the 19-electron counterpart $Mn(CO)_6^{\bullet}$ cannot be detected by the corresponding electroreduction of the carbonylmanganese(I) cation $Mn(CO)_6^+$ even at very high scan rates. Furthermore, extensive substitution of the carbonylmanganese cation with different types of ligands did not increase the lifetimes of $Mn(CO)_5L^{\bullet}$ (where L = nitriles, isonitriles, phosphites, and phosphines), with τ estimated to be less than 100 ns. Finally, the evidence for the existence of the fugitive 19-electron carbonylmanganese(0) radical is obtained indirectly by the use of the diphosphine $PPh_2CH_2CH_2PPh_2$ (DPPE) as a chelating ligand. Thus, the quantitative analysis of the cathodic reduction of *cis*-$Mn(CO)_2(DPPE)_2^+$ by digital simulation of the cyclic voltammograms, especially those generated upon repetitive cycling, reveals the presence of the reversible interchange between the 19e radical $Mn(CO)_2(\eta^2\text{-DPPE})_2^{\bullet}$ and the 17e radical $Mn(CO)_2(\eta^2\text{-DPPE})(\eta^1\text{-DPPE})^{\bullet}$. The tethered diphosphine ligand allows such an unprecedented equilibrium to be observed despite a formation constant of $K \cong 10^6$ that overwhelmingly favors the 17-electron radical.

Introduction

Electron transfer provides invaluable access to metastable and reactive intermediates produced upon the oxidation–reduction of organometallic compounds, among which are an abundant variety of stable, diamagnetic metal carbonyls.[1,2] Thus, the electron-rich anions are nucleophiles[3,4] and the electron-poor cations are electrophiles[5] that yield 17-electron and 19-electron carbonylmetal radicals, respectively, upon the electron loss from and the electron accession to their 18-electron precursors.[6] Since electron-transfer processes are becoming increasingly relevant to organometallic chemistry,[7-9] it is important to establish the temporal limits for the detection and characterization of transient 17e and 19e radicals. In this study we utilize a series of carbonylmanganese anions and cations to explore the utility of the microvoltammetric techniques[10,11] for the study of reversible electron transfer, e.g.

$$Mn(CO)_5^- \overset{-e^-}{\rightleftharpoons} \underset{17e}{Mn(CO)_5^{\bullet}} \overset{CO}{\rightleftharpoons} \underset{19e}{Mn(CO)_6^{\bullet}} \overset{+e^-}{\rightleftharpoons} Mn(CO)_6^+ \quad (1)$$

In addition, a variety of substituted phosphine (P) derivatives such as the anionic $Mn(CO)_4P^-$, $Mn(CO)_3P_2^-$, etc. and the cationic $Mn(CO)_5P^+$, $Mn(CO)_4P_2^+$, etc. are available to modulate the reversible redox potentials E° as well as the stabilities of the

(1) (a) Pickett, C. J.; Pletcher, D. *J. Chem. Soc., Dalton Trans.* **1975**, 879; **1976**, 636. (b) Pletcher, D. J. *Chem. Soc. Rev.* **1975**, *4*, 471. (c) Klingler, R. J.; Kochi, J. K. *J. Am. Chem. Soc.* **1980**, *102*, 4790.
(2) For a recent review, see: Connelly, N. G.; Geiger, W. E. *Adv. Organomet. Chem.* **1984**, *23*, 18.
(3) (a) Dessy, R. E.; Bares, L. A. *Acc. Chem. Res.* **1972**, *5*, 415. (b) Dessy, R. E.; Pohl, R. L. *J. Am. Chem. Soc.* **1968**, *90*, 2005 and references therein.
(4) Collman, J. P.; Hegedus, L. S. *Principles and Applications of Organotransition Metal Chemistry*; University Science Books: Mill Valley, CA, 1980; p 199 ff.
(5) (a) Lukehart, C. M. *Fundamental Transition Metal Organometallic Chemistry*; Brooks/Cole: Monterey, CA, 1985; p 313 ff. (b) Atwood, J. D. *Inorganic and Organometallic Reaction Mechanisms*; Brooks/Cole: Monterey, CA, 1985; Chapter 5.
(6) Kochi, J. K. *Organometallic Mechanisms and Catalysis*; Academic: New York, 1978; Chapter 8.
(7) (a) Theopold, K. *Nachr. Chem., Tech. Lab.* **1986**, *34*, 876. (b) Baird, M. C. *Chem. Rev.* **1988**, *88*, 1217.
(8) (a) Stiegman, A. E.; Tyler, D. R. *Comments Inorg. Chem.* **1986**, *5*, 215. (b) Stiegman, A. E.; Stieglitz, M.; Tyler, D. R. *J. Am. Chem. Soc.* **1983**, *105*, 6032.
(9) Chanon, M., Ed. *Paramagnetic Organometallic Species in Activation, Selectivity, Catalysis*; Reidel: Dordrecht, The Netherlands, in press.
(10) (a) Howell, J. O.; Wightman, R. M. *Anal. Chem.* **1984**, *56*, 524. (b) Howell, J. O.; Wightman, R. M. *J. Phys. Chem.* **1984**, *88*, 3915.
(11) (a) Wipf, D. O.; Kristensen, E. W.; Deakin, M. R.; Wightman, R. M. *Anal. Chem.* **1988**, *60*, 306. (b) Amatore, C. A.; Jutand, A.; Pflüger, F. *J. Electroanal. Chem. Interfacial Electrochem.* **1987**, *218*, 361.

0020-1669/89/1328-0855$01.50/0

corresponding 17-electron and 19-electron carbonylmanganese(0) radicals.[12,13]

The 17e radicals, being electron deficient and being coordinatively unsaturated, generally undergo rapid ligand substitution primarily by an associative mechanism.[14] On the other hand, the 19e radicals can be formally considered as electron-excess species and as coordinatively saturated. As such, it is not clear whether they actually are discrete intermediates (i.e., exist in bound states) or they represent activated complexes for ligand loss to afford the 17e radicals in the course of dissociative electron attachment.[15] Thus, there is only limited unambiguous experimental evidence heretofore, either direct or otherwise, that interrelates 17e and 19e carbonylmetal radicals as in the ligand interchange presented in eq 1.[16] Accordingly, our initial task is to probe directly for chemical reversibility in the electrooxidation of carbonylmanganate(−I) anions and in the electroreduction of carbonylmanganese(I) cations by microvoltammetric techniques. We then exploit mechanistic electrochemistry[19] to examine the equilibrium between 17e and 19e carbonylmanganese(0) radicals offered by the chelating diphosphine ligand $PPh_2CH_2CH_2PPh_2$ in the reduction of *cis*-$Mn(CO)_2(DPPE)_2^+$.[20]

Results and Discussion

I. Reversible Electron Transfer from Carbonylmanganate(−I) Anions. The chemical oxidation of $Mn(CO)_5^-$ and $Mn(CO)_4PPh_3^-$ by one-electron oxidants such as tropylium ion affords the dimeric $Mn_2(CO)_{10}$ and $Mn_2(CO)_8(PPh_3)_2$ in good yields.[21] Similarly, the anodic oxidation of the same carbonylmanganate(−I) anions at a platinum electrode held at constant potential yields the same results:

$$Mn(CO)_5^- \xrightarrow{0.04\ V} \tfrac{1}{2}Mn_2(CO)_{10} \quad (2)$$

$$Mn(CO)_4PPh_3^- \xrightarrow{-0.39\ V} \tfrac{1}{2}Mn_2(CO)_8(PPh_3)_2 \quad (3)$$

With both anions, coulometric measurements establish the passage of only 1 faraday of charge for the stoichiometry in eq 2 and 3. However, the oxidation of the analogous bis(phosphine)-substituted carbonylmanganate under the same conditions (i.e., tropylium or electrochemical) affords the corresponding hydridomanganese carbonyl in almost quantitative yields, i.e.

$$Mn(CO)_3(PPh_3)_2^- \xrightarrow{-0.94\ V} HMn(CO)_3(PPh_3)_2, \text{ etc.} \quad (4)$$

The difference between the oxidation stoichiometry in eq 2 and 3 and that in eq 4 can be reconciled with the rates of dimerization of the carbonylmanganese(0) intermediates. Thus, the second-order rate constants[22] for $Mn(CO)_5^\bullet$ and $Mn(CO)_4PPh_3^\bullet$, k_d = 9×10^8 and 1×10^7 M^{-1} s^{-1}, respectively, approach the diffusion-controlled limit to favor dimerization, as shown in Scheme I. On the other hand, the sterically encumbered bis-substituted radical $Mn(CO)_3(PPh_3)_2^\bullet$ is persistent and shows no or limited inclination to dimerize,[23] and its only recourse is hydrogen atom transfer to produce the manganese hydride according to Scheme II.[13] The facility of the follow-up steps in eq 6 and 9 largely determines whether the chemical reversibility of electron transfer in eq 5 and 7, respectively, can be observed by cyclic voltammetric techniques.[24]

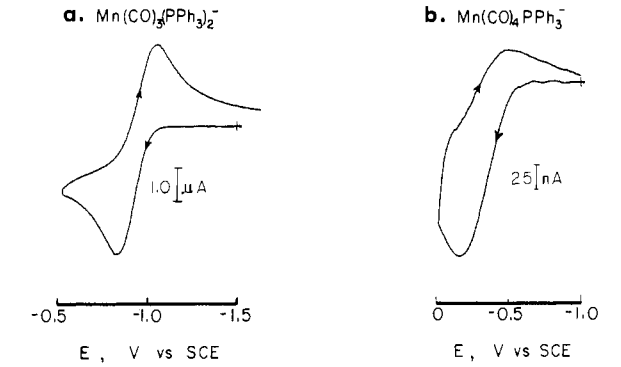

Figure 1. Initial positive-scan cyclic voltammograms of (a) 1.0×10^{-2} M $Mn(CO)_3(PPh_3)_2^-$ at v = 0.5 V s^{-1} with a Pt macroelectrode (r = 0.5 mm) and (b) 1.0×10^{-2} M $Mn(CO)_4(PPh_3)^-$ at v = 4000 V s^{-1} with a Pt microelectrode (r = 5 μm) in MeCN containing 0.3 M $TBA^+PF_6^-$ at 23 °C.

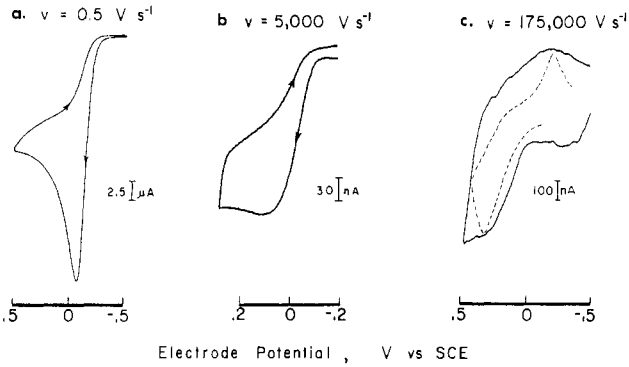

Figure 2. Initial positive-scan cyclic voltammograms of 1.0×10^{-2} M $Mn(CO)_5^-$ at (a) v = 0.5 V s^{-1} with a Pt macroelectrode, (b) v = 5000 V s^{-1} with a Pt microelectrode, and (c) v = 175 000 V s^{-1} with a Pt microelectrode in MeCN containing 0.3 M $TBA^+PF_6^-$ at 23 °C. For an explanation of dashed curve, see the Experimental Section.

Scheme I

$$Mn(CO)_5^- \overset{-e^-}{\rightleftharpoons} Mn(CO)_5^\bullet \quad (5)$$

$$2Mn(CO)_5^\bullet \xrightarrow{k_d} [Mn(CO)_5]_2 \quad (6)$$

Scheme II

$$Mn(CO)_3P_2^- \overset{-e^-}{\rightleftharpoons} Mn(CO)_3P_2^\bullet \quad (7)$$

$$2Mn(CO)_3P_2^\bullet \leftrightarrows [Mn(CO)_3P_2]_2 \quad (8)$$

$$Mn(CO)_3P_2^\bullet + SH \rightarrow HMn(CO)_3P_2 + S^\bullet, \text{ etc.} \quad (9)$$

The reversible cyclic voltammograms in Figure 1 demonstrate that electron-transfer reversibility for the persistent radical $Mn(CO)_3(PPh_3)_2^\bullet$ is attained with a cathodic/anodic peak current

(12) Note that the reduction of $Mn(CO)_6^+$ to $Mn(CO)_5^-$ in eq 12 requires two electrons. (a) Narayanan, B. A.; Amatore, C.; Kochi, J. K. *Organometallics* **1987**, *6*, 129. (b) Kuchynka, D. J.; Amatore, C.; Kochi, J. K. *Inorg. Chem.* **1986**, *25*, 4087.
(13) (a) Amatore, C.; Kuchynka, D. J.; Kochi, J. K. *J. Electroanal. Chem. Interfacial Electrochem.* **1988**, *241*, 181. (b) Kuchynka, D. J.; Amatore, C.; Kochi, J. K. *J. Organomet. Chem.* **1987**, *328*, 133.
(14) (a) Herrinton, T. R.; Brown, T. L. *J. Am. Chem. Soc.* **1985**, *107*, 5700. (b) Fox, A.; Malito, J.; Poe, A. *J. Chem. Soc., Chem. Commun.* **1981**, 1052. (c) Shi, Q. Z.; Richmond, T. G.; Trogler, W. C.; Basolo, F. *J. Am. Chem. Soc.* **1982**, *104*, 4032. See however: Kowaleski, R. M.; Basolo, F.; Trogler, W. C. *J. Am. Chem. Soc.* **1986**, *108*, 6046.
(15) See Discussion in ref 8 and 12. Astruc, D. *Chem. Rev.* **1988**, *88*, 1189.
(16) For example in the cyclopentadienyl and related derivatives of metal carbonyls,[17] there is some ambiguity of $\eta^{3,4}$ bonding (i.e., Cp ring slippage)[18] in the absence of X-ray crystallographic structures of the 19e radicals.
(17) See e.g.: Philbin, C. E.; Granatir, C. A.; Tyler, D. R. *Inorg. Chem.* **1986**, *25*, 4886.
(18) Cf.: Rerek, M. E.; Basolo, F. *J. Am. Chem. Soc.* **1984**, *106*, 5908.
(19) Heinze, J. *Angew. Chem., Int. Ed. Engl.* **1984**, *23*, 831. See also ref 1b.
(20) $PPh_2CH_2CH_2PPh_2$ hereafter referred to as DPPE.
(21) Armstead, J. A.; Cox, D. J.; Davis, R. *J. Organomet. Chem.* **1982**, *236*, 213.
(22) Walker, H. W.; Herrick, R. S.; Olsen, R. J.; Brown, T. L. *Inorg. Chem.* **1984**, *23*, 3748.
(23) McCullen, S. B.; Brown, T. L. *J. Am. Chem. Soc.* **1982**, *104*, 7496. See also ref 13 and: Kidd, D. R.; Cheng, C. P.; Brown, T. L. *J. Am. Chem. Soc.* **1978**, *100*, 1978. Brown, T. L. *Ann. N.Y. Acad. Sci.* **1980**, *80*, 333.
(24) (a) In cyclic voltammetry, only the observation of the peak current on the reverse scan is needed for chemical reversibility. (b) In this situation, the reversible potential E° is adequately expressed as the average of the anodic and cathodic peak potentials, $(E_a + E_c)/2$, as described in ref 25.
(25) Howell, J. O.; Goncalves, J. M.; Amatore, C.; Klasinc, L.; Wightman, R. M.; Kochi, J. K. *J. Am. Chem. Soc.* **1984**, *106*, 3968.

Table I. Microvoltammetric Determination of Oxidation Potentials of Carbonylmanganate(–I) Anions[a]

anion	E°, V vs SCE	v, V s^{-1}
$Mn(CO)_5^-$	0.084	40 000
	0.081	80 000
	0.084	120 000
	0.090	175 000
av	0.085 ± 0.005	
$Mn(CO)_4PPh_3^-$	−0.408	1 000
	−0.406	2 000
	−0.400	4 000
	−0.392	6 000
av	−0.403 ± 0.009	

[a] In 1.0×10^{-2} M solutions in acetonitrile containing 0.1 M tetra-*n*-butylammonium hexafluorophosphate at 23 °C with a Pt microelectrode (r = 5 μm).

Table II. Reversible Potentials E° for Carbonylmanganate(–I) Anions from Cyclic Voltammetry[a]

carbonylmanganate	v,[b] V s^{-1}	E°,[c] V vs SCE
$Mn(CO)_5^-$	175000[d]	+0.08
$Mn(CO)_4PPh_3^-$	2000[d]	−0.40
$Mn(CO)_3(PPh_3)_2^-$	>0.02[e]	−0.94
$Mn(CO)_2(DPPE)_2^-$	>0.02[e]	−1.44

[a] In 1.0×10^{-2} M solutions in acetonitrile containing 0.1 M tetra-*n*-butylammonium hexafluorophosphate at 23 °C unless indicated otherwise. [b] Scan rate to attain $i_c/i_a \approx 0.5$. [c] $E^\circ = (E_a + E_c)/2$ as described in ref 24. [d] With Pt microelectrode (r = 5 μm). [e] With conventional Pt electrode (r = 0.5 mm) in THF containing 0.5 M $TBA^+PF_6^-$.

ratio of i_c/i_a = 1.0 (theoretical) at a scan rate of v = 0.5 V s^{-1}, whereas the more transient radical $Mn(CO)_4PPh_3^\bullet$ requires a 10^4 faster scan rate to achieve reversibility. By comparison the parent manganese carbonyl $Mn(CO)_5^\bullet$ is the more transient radical, and the initial positive-scan cyclic voltammogram in Figure 2a is totally irreversible at the conventional scan rate of v = 0.5 V s^{-1}. Moreover, the cyclic voltammogram is still irreversible at v = 5000 V^{-1} with a platinum microelectrode, as shown by the absence of a clearly defined cathodic peak current on the return scan in Figure 2b. Indeed, a scan rate in excess of 40 000 V s^{-1} is required before the cathodic peak current can be simultaneously discerned. The reversible cyclic voltammogram at v = 175 000 V s^{-1} in Figure 2c with the peak broadening arising from uncompensated iR drop[26] and the nonfaradaic charging current is shown by comparison with the normal cyclic voltammogram represented by the dashed curve. The arithmetic average of the anodic and cathodic peak potentials $(E_a + E_c)/2$ obtained in this manner represents a reliable measure of the reversible potential E° for the redox couple.[24b] The constancy of E^0 at the various scan rates in Table I is an indication of the reproducibility of the microvoltammetric method for $Mn(CO)_5^-$ and $Mn(CO)_4PPh_3^-$.

The chemically reversible oxidations of the various carbonylmanganate(–I) anions yield the values of the redox potential E_2° in Table II. For the EC process depicted in Scheme I, the second-order dimerization rate constant k_d can be calculated from a knowledge of the ratios of the cathodic and anodic peak currents i_c/i_a at various scan rates according to the method of Nicholson and co-workers.[27] Owing to the well-behaved values of i_c/i_a at CV scan rates between 1000 and 6000 V s^{-1} for $Mn(CO)_4PPh_3^-$, we successfully extracted the bimolecular rate constant $k_d = 1.4 \times 10^7$ M^{-1} s^{-1} for the dimerization of $Mn(CO)_4PPh_3^\bullet$ (see Experimental Section):

$$2Mn(CO)_4PPh_3^\bullet \xrightarrow{k_d} Mn_2(CO)_8(PPh_3)_2 \qquad (10)$$

This value is in excellent agreement with the rate constant (vide supra) evaluated from the flash photolysis of $Mn_2(CO)_8(PPh_3)_2$ by Brown and co-workers.[22] For $Mn(CO)_5^-$, our limited observation of well-behaved peak current ratios owing to problems with uncompensated ohmic drop and large charge currents at the requisite higher scan rates necessitated an estimate for $Mn(CO)_5^\bullet$ of $k_d = 7 \times 10^8$ M^{-1} s^{-1} based on a current ratio of unity at v = 175 000 V s^{-1} (Figure 2; see Experimental Section). Nonetheless this value is clearly within experimental uncertainty the same as $k_d = 9 \times 10^8$ M^{-1} s^{-1} from the flash photolysis of $Mn_2(CO)_{10}$.[22]

The ready chemical reversibility of disubstituted carbonylmanganates $Mn(CO)_3P_2^-$ (where P = alkylphosphines and alkyl phosphites) is shown by the well-behaved cyclic voltammograms with i_c/i_a = 1.0 that are easily attainable even at sweep rates of v = 0.050 V s^{-1},[13] e.g.

$$Mn(CO)_3[P(OPh)_3]_2^- \overset{-0.55\ V}{\rightleftharpoons} Mn(CO)_3[P(OPh)_3]_2^\bullet + e^- \qquad (11)$$

The trend in the values of the reversible oxidation potentials in Table III largely follows the σ-donor properties of the phosphine ligand as evaluated by the pK_a of the conjugate acid.[28] However, the necessity for including a different correlation for phosphite ligands in Figure 3 suggests that π-acidity in back-bonding is also a contributing factor in E°. Moreover, the effects of additional phosphine ligands in the heavily substituted $Mn(CO)_2(DPPE)_2^-$ are reflected in a highly reversible cyclic voltammogram and the most negative value of E° = −1.45 V.[29]

Table III. Ligand Dependence of the Reversible Potentials for the Carbonylmanganate(–I) Anions $Mn(CO)_3P_2^-$[a]

ligand P	E°, V vs SCE	ligand P	E°, V vs SCE
Ph_3P	−0.94	$(n\text{-}Bu)_3P$	−1.20
$(PhO)_3P$	−0.55	$(i\text{-}PrO)_3P$	−0.81
$(o\text{-}CH_3C_6H_4O)_3P$	−0.59	$(i\text{-}Pr)_3P$	−1.22
$PPh_2CH_2CH_2PPh_2$	−1.07		

[a] By cyclic voltammetry at v = 0.5 V s^{-1} in THF containing 0.3 M $TBA^+PF_6^-$ with a platinum electrode at 23 °C.

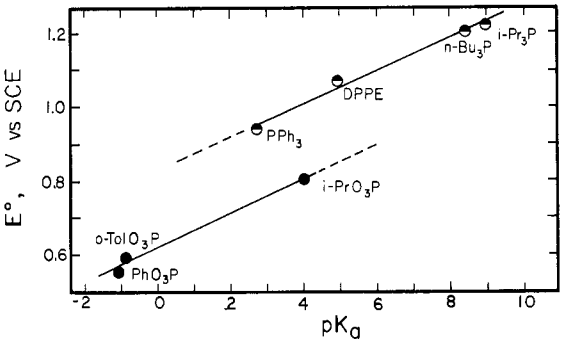

Figure 3. Correlation of the reversible oxidation potential E° for $Mn(CO)_3P_2^-$ and the pK_a of HP^+ for the alkylphosphine and alkyl phosphite ligands (P) indicated.

II. Electroreduction of Carbonylmanganese(I) Cations. The cathodic reduction of the carbonylmanganese(I) cation $Mn(CO)_6^+$ occurs with the uptake of 1.4 faradays of charge and the evolution of 1.0 mol of carbon monoxide according to the partial stoichiometry in eq 12.[12] The carbonylmanganese products in eq

$$Mn(CO)_6^+ \xrightarrow{-1.20\ V} CO + [Mn(CO)_5^- + Mn_2(CO)_{10}] \qquad (12)$$

12 derive most likely via the 17e radical according to Scheme III.[30]

Scheme III

$$Mn(CO)_6^+ \overset{e^-}{\rightleftharpoons} Mn(CO)_6^\bullet \qquad (13)$$

$$Mn(CO)_6^\bullet \rightarrow CO + Mn(CO)_5^\bullet, \text{ etc.} \qquad (14)$$

(26) See, e.g., Wightman et al. in ref 11a and: Andrieux, C. P.; Garreau, D.; Hapiot, P.; Pinson, J.; Saveant, J. M. *J. Electroanal. Chem. Interfacial Electrochem.* **1988**, *243*, 321.
(27) Olmstead, M. L.; Hamilton, R. G.; Nicholson, R. S. *Anal. Chem.* **1969**, *41*, 260.
(28) See: (a) Zizelman, P. M.; Amatore, C.; Kochi, J. K. *J. Am. Chem. Soc.* **1984**, *106*, 3771. (b) Golovin, M. N.f Rahman, M. M.; Belmonte, J. E.; Giering, W. P. *Organometallics* **1985**, *4*, 4981.
(29) Kuchynka, D. J.; Kochi, J. K. *Inorg. Chem.* **1988**, *27*, 2574.

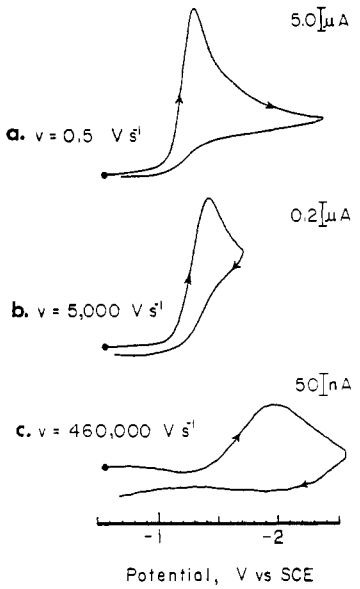

Figure 4. Initial negative-scan cyclic voltammograms of 1.0×10^{-2} M $Mn(CO)_6^+$ at (a) $v = 0.5$ V s^{-1} with a Pt macroelectrode, (b) $v = 5000$ V s^{-1} with a Pt microelectrode, and (c) $v = 460000$ V s^{-1} with a Pt microelectrode in acetonitrile containing 0.1 M $TBA^+PF_6^-$ at 23 °C.

Table IV. Microvoltammetry of Carbonylmanganese(I) Cations[a]

carbonylmanganese(I)	v,[b] V s^{-1}	E_c,[c] V vs SCE	τ,[d] μs
$Mn(CO)_6^+BF_4^-$	460 000	−1.27	0.06
$Mn(CO)_6^+BF_4^-$[e]	460 000	−1.27	0.06
$Mn(CO)_5PPh_3^+BF_4^-$	200 000	−1.29	0.13
$Mn(CO)_3(NCCH_3)_3^+BF_4^-$	200 000	−1.87	0.13
trans-$Mn(CO)_2(DPPE)_2^+PF_6^-$	225 000	−1.94	0.11
cis-$Mn(CO)_2(CNCH_3)_4^+PF_6^-$	150 000	−2.48	0.17
$Mn(CNC_6H_4CH_3)_6^+PF_6^-$	170 000	−2.41	0.15
cis-$Mn(CO)_2[P(OMe)_3]_4^+BF_4^-$	225 000	−2.10	0.11

[a] In 1.0×10^{-2} M solutions in acetonitrile containing 0.1 M tetra-*n*-butylammonium hexafluorophosphate at 23 °C with a Pt microelectrode ($r = 5$ μm). [b] Irreversible cyclic voltammogram at the v value indicated. [c] Irreversible cathodic peak potential at $v = 0.5$ V s^{-1}. [d] Estimated upper limit to lifetime of 19e radical; see text. [e] In the presence of 1 atm of carbon monoxide.

We accordingly examined the cyclic voltammetric behavior of $Mn(CO)_6^+$ for signs of chemical reversibility. The initial positive-scan cyclic voltammogram at $v = 0.5$ V s^{-1} with a conventional platinum electrode is totally irreversible (Figure 4a), showing only the cathodic peak for the reduction of $Mn(CO)_6^+$. Calibration of the peak current i_c with a ferrocene standard[31] indicates that the cathodic wave corresponds to an uptake of 1.3 faradays of charge, in agreement with the coulometric results (vide supra). The cyclic voltammogram at $v = 5000$ V s^{-1} with a platinum microelectrode (radius 5 μm) in Figure 4b is fundamentally unchanged relative to that at $v = 0.5$ V s^{-1}. Furthermore, even at the fastest practicable limit[32] of $v = 460000$ V s^{-1}, no anodic peak current could be detected on the return scan (see Figure 4c). From results such as these, we estimate the first-order rate of decomposition of the 19-electron $Mn(CO)_6^\bullet$ to be $>10^7$ s^{-1}.

In order to determine whether the presence of different ligands would otherwise stabilize the 19-electron radicals, we prepared the various substituted carbonylmanganese(I) cations in Table IV.[13] Although large changes in the cathodic peak potentials E_c were indeed induced by structurally different types of ligands, we found no evidence for chemical reversibility in electron transfer to carbonylmanganese cations, even at the enhanced scan rates

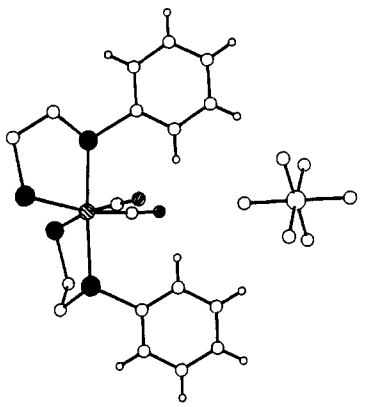

Figure 5. ORTEP diagram of *cis*-$Mn(CO)_2(DPPE)_2^+AsF_6^-$ showing the ion-pair interaction. Note only two of the eight phenyl groups on the DPPE ligands are shown for clarity.

listed in Table IV. In every case we estimate the lifetime of the 19e carbonylmanganese(0) radicals to be less than 100 ns when they are limited by the dissociative loss of ligand such as that depicted in Scheme IV.[33] For this reason, we next turned to the carbonylmanganese(I) cation that contained the pair of chelating diphosphine ligands $PPh_2CH_2CH_2PPh_2$ (DPPE) since such difunctional ligands were found in an earlier study to stabilize other types of reduced carbonylmetals.[34]

Scheme IV

$$Mn(CO)_5P^+ \overset{e^-}{\rightleftharpoons} Mn(CO)_5P^\bullet \qquad (15)$$

$$Mn(CO)_5P^\bullet \xrightarrow{<10^{-7}\ s} Mn(CO)_5^\bullet + P \qquad (16)$$

III. Reversible Interchange of 19e and 17e Radicals during the Reduction of the Bis-Chelated $Mn(CO)_2(DPPE)_2^+$. In order to optimize the equilibration of 19e and 17e organometallic radicals, we focused on a bis-chelated carbonylmanganese(0) radical in which the tethering of the difunctional ligand would also favor the reversible interchange, e.g.

19e 17e (17)

The equilibrium between such chelated radicals is expected to be especially facile when the reversible interchange in eq 17 involves no or minimal structural changes. As such, we are fortunate that the recent synthesis[35] of *cis*-$Mn(CO)_2(DPPE)_2^+$, illustrated in Figure 5 and designated hereafter simply as I, provided the opportunity to generate directly the isomeric 19e radical required for eq 17 in the following way.

The preparative-scale electroreduction of *cis*-$Mn(CO)_2(DPPE)_2^+$ (I) at a controlled potential of −2.0 V in acetonitrile containing 0.1 M TBAP as the supporting electrolyte was characterized by the uptake of 2.0 faradays of charge per mole of cation to produce the *cis*-dicarbonylmanganate(−I) complex II in eq 18.[36]

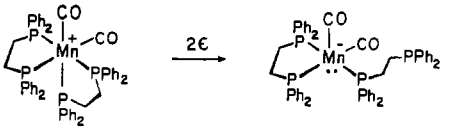

I II (18)

The 2e reduction of the cation I was accompanied by the dramatic color change of the pale yellow solution to the dark red anion II

(30) Lee, K. Y.; Kuchynka, D. J.; Kochi, J. K. *Organometallics* **1987**, *6*, 1886.
(31) Gagne, R. R.; Koval, C. A.; Lisensky, G. C. *Inorg. Chem.* **1980**, *19*, 2854.
(32) Owing to limited, measurable cathodic currents.
(33) For the competitive loss of CO or P in eq 16, see ref 12b.
(34) Richmond, M. G.; Kochi, J. K. *Inorg. Chem.* **1986**, *25*, 656. Richmond, M. G.; Kochi, J. K. *Organometallics* **1987**, *6*, 254.
(35) Kuchynka, D. J.; Kochi, J. K. *Organometallics* **1989**, *8*, 677.
(36) For details of the stoichiometry and all the products of I, see the Experimental Section.

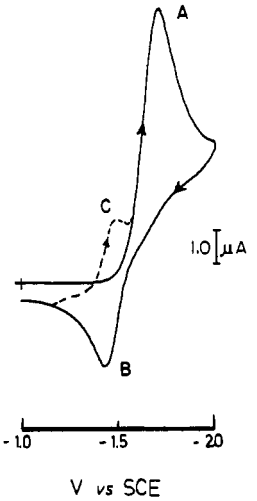

Figure 6. Initial negative-scan cyclic voltammogram at 23 °C of 5×10^{-3} M *cis*-$Mn(CO)_2(DPPE)_2^+AsF_6^-$ in THF containing 0.3 M TBAP at v = 0.5 V s^{-1} with a Pt macroelectrode. The dashed curve shows the cathodic wave on the return scan.

and the concomitant IR change in the carbonyl region from ν_{CO} = 1894 and 1950 cm^{-1} for I to ν_{CO} = 1710 and 1766 cm^{-1} for II.[29] The transient electrochemical behavior accompanying the 2e reduction of *cis*-$Mn(CO)_2(DPPE)_2^+$ in eq 18 was examined by cyclic voltammetry. The initial negative-scan cyclic voltammogram of I in Figure 6 shows an irreversible cathodic wave A with the peak potential E_c = −1.71 V corresponding to a 2e reduction of I, as calibrated with a ferrocene standard.[31] The formation of the anion II for eq 18 is shown in the cyclic voltammogram (Figure 6) by the presence of the anodic wave B on the return positive scan. The latter with E_a = −1.39 V represents the oxidation of the anion $Mn(CO)_2(DPPE)_2^-$(II) to the corresponding 17-electron radical (hereafter referred to simply as 17e), i.e.

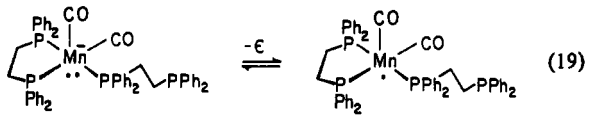

(19)

II 17e

The anodic wave B is the same as that in a cyclic voltammogram obtained from the anodic oxidation of authentic anion II prepared independently.[29] Furthermore, its reversible character is shown by the presence of the dashed cathodic wave C on the reverse negative scan. It is important to note that wave C occurs at a potential of E_c = −1.52 V, which is substantially more positive than that of wave A at E_c = −1.71 V for the initial reduction of the cation I. As a result, the reduction of 17e is also included in the 2e cathodic wave A, which remained chemically irreversible even at CV scan rates exceeding 100 000 V s^{-1}, easily achieved with the platinum microelectrode (vide supra).

The transient electrochemical behavior of I in Figure 6 is akin to that of the isomeric *trans*-$Mn(CO)_2(DPPE)_2^+$, for which the mechanism of the 2e reduction was successfully delineated as the ECE-Disp process.[29] As applied to the closely related *cis*-$Mn(CO)_2(DPPE)_2^+$, the corresponding ECE-Disp mechanism for cation reduction is as shown in Scheme V.

Scheme V

$$I \xrightarrow{e^-} 19e \qquad (20)$$

$$19e \xrightarrow{k_f} 17e \qquad (21)$$

$$17e \rightleftharpoons II \qquad (22)$$

$$I + II \underset{k_d}{\overset{k_{et}}{\rightleftharpoons}} 19e + 17e \qquad (23)$$

According to the ECE-Disp mechanism in Scheme V, the repeated cycling of the potential scans should lead to a steady-state

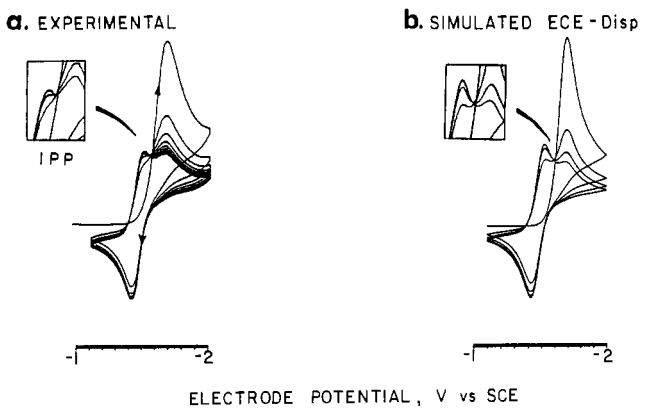

Figure 7. (a) Initial negative-scan (15-cycle) cyclic voltammograms of 5×10^{-3} M *cis*-$Mn(CO)_2(DPPE)_2^+AsF_6^-$ in THF containing 0.3 M TBAP at v = 0.4 V s^{-1}. (b) Simulated (4-cycle) cyclic voltammograms based on the ECE-Disp mechanism, as described in the text.

cyclic voltammogram like that shown in Figure 7a. Thus after only ~5 cycles, the cathodic wave A for *cis*-$Mn(CO)_2(DPPE)_2^+$ is markedly diminished and the B/C couple is dominant. The isopotential point (IPP being akin to isosbestic point in spectroscopy)[37] at −1.64 V indicated that one electroactive species (I) was quantitatively converted to the other (II), the sum of the reactant and the product concentrations thus remaining constant throughout the repetitive scans. The essential correctness of the ECE-Disp formulation for *cis*-$Mn(CO)_2(DPPE)_2^+$ is confirmed by the computer simulation of the cyclic voltammogram in Figure 7b over a sequence of four repetitive cycles. The CV simulations were carried out with Feldberg's finite difference (digital) method[38,39] by use of optimized electrochemical parameters stemming from the previous study of *trans*-$Mn(CO)_2(DPPE)_2^+$,[29,40] as described in the Experimental Section. Thus for the kinetics, the first-order rate constant for the 19e/17e conversion in eq 21 was set as $k_f = 1 \times 10^6$ s^{-1} to accord with the microvoltammetric results;[41] the optimized rate constants for the electron transfer and disproportionation in eq 23 were $k_{et} = 2.0 \times 10^2$ M^{-1} s^{-1} and k_d = 20 M^{-1} s^{-1}. Indeed, the rapidity of such an ion-pair annihilation can be independently demonstrated by mixing solutions of *cis*-$Mn(CO)_2(DPPE)_2^+AsF_6^-$ and *mer*-$Mn(CO)_2(DPPE)_2^-$ Bu_4N^+ whereupon the ESR spectrum at $\langle g \rangle$ = 2.025 taken immediately of the 17e radical was the same as that obtained from the anodic oxidation of II.[29]

Although the ECE-Disp mechanism correctly predicts the rapid falloff of the CV wave A, a closer scrutiny of Figure 7b revealed the following three important discrepancies from the experimental CV in Figure 7a. (a) The height of the cathodic wave A on the fourth cycle is less than that of wave C. (For details, see the insets.) (b) The height of the cathodic wave C is larger on all cycles. (c) The IPP is positioned at a lower current between peaks C and A. The analysis of the behavior (a)–(c) indicates that the

(37) (a) Gaudiello, J. G.; Wright, T. C.; Jones, R. A.; Bard, A. J. *J. Am. Chem. Soc.* **1985**, *107*, 888. See also: (b) Untereker, D. F.; Bruckenstein, S. *Anal. Chem.* **1972**, *44*, 1009. Untereker, D. F.; Bruckenstein, S. *J. Electroanal. Chem. Interfacial Electrochem.* **1974**, *57*, 77.
(38) Feldberg, S. W. In *Electroanalytical Chemistry*; Bard, A. J., Ed.; Dekker: New York, 1969; Vol. 3, p 199.
(39) Feldberg, S. W. In *Computer Applications in Analytical Chemistry*; Mark, H. B., Ed.; Dekker: New York, 1972; p 185.
(40) Note that the rate constants used here differ slightly from the earlier ones,[29] since the latter were based on the approximation that electron transfer in eq 23 produced a pair of 17e species (owing to the rapid isomerization of 19e in eq 21).
(41) (a) Nicholson, R. A.; Shain, I. *Anal. Chem.* **1964**, *36*, 706. (b) Nicholson, R. A.; Shain, I. *Anal. Chem.* **1965**, *37*, 178. (c) Saveant, J. M. *Electrochim. Acta* **1967**, *12*, 753.
(42) For the successful application of CV simulation, see: (a) Hershberger, J. W.; Klingler, R. J.; Kochi, J. K. *J. Am. Chem. Soc.* **1983**, *105*, 61. (b) Bockman, T. M.; Kochi, J. K. *J. Am. Chem. Soc.* **1987**, *109*, 7725.
(43) Furthermore in the simulation, the initial CV was found to go through the IPP, clearly at variance from the experimental CV. This is not an artifact of the simulation and was observed earlier by Gaudiello et al.[37a]

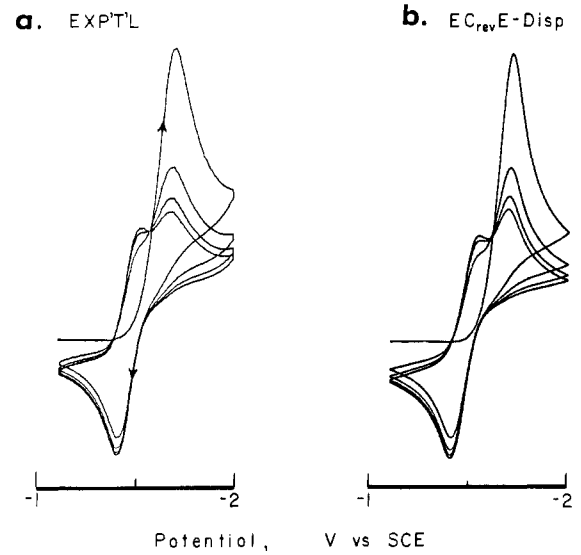

Figure 8. (a) Initial negative-scan (4-cycle) cyclic voltammograms of 5 × 10^{-3} M *cis*-$Mn(CO)_2(DPPE)_2^+AsF_6^-$ in THF containing 0.3 M TBAP at v = 0.4 V s^{-1}. (b) Simulated (4-cycle) cyclic voltammograms based on the $EC_{rev}E$-Disp mechanism in Scheme VI.

17e radical is actually undergoing a reaction that reduces its concentration and simultaneously increases the concentration of the cation I relative to the ECE-Disp simulation. An obvious remedy to this kinetics situation is to include reversibility in the formation of the 17e radical from the cation I, viz.

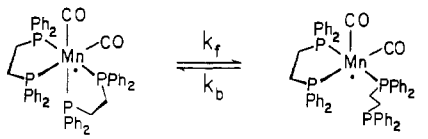

(24)

Inclusion of this reversible interchange to generate the $EC_{rev}E$-Disp mechanism in Scheme VI resulted in the CV simulation presented in Figure 8. The excellent agreement of the simulated cyclic voltammogram (Figure 8b) with the experimental one (Figure 8a) was carried out with the same optimized rate constants and $k_f = 1 \times 10^6$ s^{-1} and $k_b = 3.5$ s^{-1}.[44] Inspection of the simulated CV (Figure 8b) in the region of the IPP now reveals its position in both the current and potential scales to be in perfect agreement with the experimental curves (Figure 8a). Furthermore, there are two critical features, namely (a) the rate of depletion of the cation I (wave A) upon recycling and (b) the passage of the first scan at a point negative of IPP, that are both seen to match the experimental trace.[37a] At first glance the value of $k_b = 3.5$ s^{-1} may seem to be unusually small to have any drastic effect on the CV traces. However, cognizance must be taken of the fact that such a 17e/19e conversion always occurs in a potential region ≤ -1.45 V (i.e., $E_2°$ for the oxidation of anion II), which is ~150 mV more positive than $E_1° = -1.61$ V for the reduction of cation I! As a result, the 19e radical is immediately oxidized at the electrode surface and the reversible interchange in eq 26 (however slow) is tantamount to the spontaneous regeneration of the cation I. The validity of this analysis is underscored in Figure 9 by the excellent agreement between experimental and simulated steady-state cyclic voltammograms after 15 cycles based on the ECE-Disp mechanism in Scheme VI.

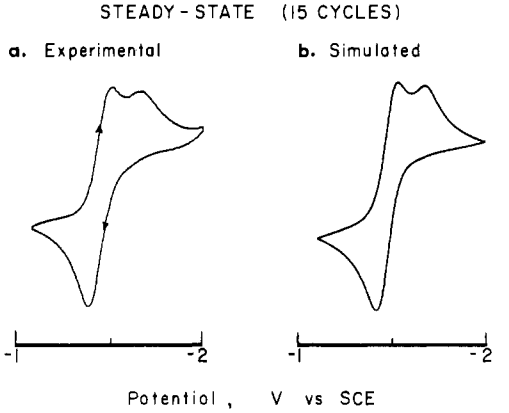

Figure 9. Comparison of the (a) experimental and (b) simulated steady-state cyclic voltammograms after 15 cycles of *cis*-$Mn(CO)_2(DPPE)_2^+$ based on the $EC_{rev}E$-Disp mechanism (see text).

Scheme VI

$$I \xrightarrow{e^-} 19e \tag{25}$$

$$19e \underset{k_b}{\overset{k_f}{\rightleftharpoons}} 17e \tag{26}$$

$$17e \overset{e^-}{\rightleftharpoons} II \tag{27}$$

$$I + II \rightleftharpoons 19e + 17e \tag{28}$$

It is singularly noteworthy that the optimized magnitudes of the first-order rate constants of $k_b = 3.5$ s^{-1} relative to $k_f = 10^6$ s^{-1} in eq 26 indicate an "equilibrium" constant $K \cong 10^6$ that favors the *opened* 17e radical over the *closed* 19e counterpart.[48] Therefore, it is not surprising that we were unable to observe the reversible interchange between 17e and 19e radicals during the reduction of the nonchelated carbonylmanganese(I) cations such as those listed in Table IV. However short their lifetime, we conclude that 19e carbonylmanganese(0) radicals are discrete intermediates as distinguished from activated complexes located at maxima of potential energy surfaces.

IV. Comments on the Annihilation Rates of Isomeric $Mn(CO)_2(DPPE)^+$/$Mn(CO)_2(DPPE)_2^-$ Ion Pairs. Critical to the successful mechanistic elucidation of the reduction of the cationic $Mn(CO)_2(DPPE)_2^+$ in Scheme VI is the facile annihilation of the ion pair according to eq 28. For a reversible process, the second-order rate constants are related to the driving force by the equilibrium relationship[49] shown in eq 29, in which the magnitude

$$RT \ln (k_{et}/k_d) = n\mathcal{F}(\Delta E°) \tag{29}$$

of $\Delta E°$ is given by $E_1° - E_2° = 0.11$ V and k_{et} is the optimized second-order rate constant for electron transfer with a value of 2×10^2 M^{-1} s^{-1}. The calculated value from eq 29 of the second-order rate constant for radical disproportionation of $k_d = 0.4$

(44) The four-cycle CV traces in Figure 8a could only be reproduced after the Pt electrode was polished, which indicated a slight pollution. The near-Nernstian behavior of the ferrocene/ferrocenium couple[31] in the same CV cell exhibited a peak separation $E_a - E_c \cong 120$ mV in THF (0.3 M TBAP) at 400 mV s^{-1}, indicating substantial ohmic drop.[45] These effects can lead to the wave broadening in Figure 8a, especially when k_s is slow (see ref 46c). Our inability to simulate exactly the gap between the feet of waves A and B may also be due to wave broadening caused by electrode pollution and/or ohmic drop, especially in systems in which k_s is rather slow.[46]

(45) Imbeaux, J. C.; Saveant, J. M. *J. Electroanal. Chem. Interfacial Electrochem.* **1970**, *28*, 325.

(46) For example, see: (a) Bond, A. M.; Colton, R.; McDonald, M. E. *Inorg. Chem.* **1978**, *17*, 2842. (b) Reference 13b. (c) The dependence of E_c on v for I was 75 mV/log unit of v rather than the 29 mV/log unit of v predicted for Nernstian charge transfer.[47]

(47) Parker, V. D. In *Electroanalytical Chemistry*; Bard, A. J., Ed.; Dekker: New York, 1986; Vol. 14.

(48) (a) For the square-pyramidal structure of the 17e radical, see ref 29. With other systems, both theory (Hoffman, R.; Rossi, A. R. *Inorg. Chem.* **1975**, *14*, 365. Elian, M.; Hoffman, R. *Inorg. Chem.* **1975**, *14*, 1058.) and experiment (Symons, M. C. R.; Sweany, R. L. *Organometallics* **1982**, *1*, 834. Church, S. P.; Poliakoff, R. L.; Timney, J. A.; Turner, J. J. *J. Am. Chem. Soc.* **1981**, *103*, 7515. Kidd, D. R.; Cheng, C. P.; Brown, T. L. *J. Am. Chem. Soc.* **1978**, *100*, 4103.) also favor the square-pyramidal structure. (b) For the fluxional behavior of the d^9 complex $Rh(DPPE)_2$, see: Mueller, K. T.; Kunin, A. J.; Greiner, S.; Henderson, T.; Kreilick, R. W.; Eisenberg, R. *J. Am. Chem. Soc.* **1987**, *109*, 6313.

(49) Bard, A. J.; Faulkner, L. R. *Electroanalytical Methods*; Wiley: New York, 1980. The approximation ignore the follow-up reactions (vide supra).

M^{-1} s^{-1} is indeed within the range predicted by the CV simulation (see Figure 8b).[50]

The rate of ion-pair annihilation of *cis*-$Mn(CO)_2(DPPE)_2^+$ by $Mn(CO)_2(DPPE)_2^-$ (II) with a second-order rate constant k_{et} = 2×10^2 M^{-1} s^{-1} is a factor of 6 faster than the annihilation of the isomeric *trans*-$Mn(CO)_2(DPPE)_2^+$ with the same anion (k_{et} = 35 M^{-1} s^{-1}) examined earlier.[29] Such a trend in the electron-transfer rates parallels the difference in the driving force of 3.4 kcal mol^{-1} evaluated from the reduction potentials of $E_1° = -1.61$ and -1.76 V for *cis*- and *trans*-$Mn(CO)_2(DPPE)_2^+$, respectively. The latter together with the value of $E_2° = -1.45$ V for the oxidation of the anionic $Mn(CO)_2(DPPE)_2^-$ indicates that the reductions of *cis*- and *trans*-$Mn(CO)_2(DPPE)_2^+$ both by II have driving forces of 3.7 and 7.1 kcal mol^{-1}, respectively. These driving forces are exergonic and considerably more favorable than those involved in the electron-transfer reactions of the simple, monosubstituted carbonylmanganese cations $Mn(CO)_5L^+$ and anions $Mn(CO)_4P^-$ (where L and P are both monodentate phosphines and phosphites) that we examined previously.[12] Nonetheless the rate constants k_{et} for *cis*- and *trans*-$Mn(CO)_2(DPPE)_2^+$ with $Mn(CO)_2(DPPE)_2^-$ are considerably slower than those qualitatively observed between $Mn(CO)_5L^+$ and $Mn(CO)_4P^-$.[30] Such large rate differences that belie thermodynamics can be attributed to steric hindrance in the tetrasubstituted carbonylmanganese cations and anions that is absent in the simpler ions. Indeed, the ORTEP diagram shown in Figure 5 visually underscores the limited access to the manganese centers arising from the ligand encumbrance. Such structural effects, even in these apparently outer-sphere electron transfers, merit a further quantitative evaluation as in the application of Marcus theory.[51]

Experimental Section

Materials. Manganese decacarbonyl (Pressure Chemical Co.) and triphenylmethyl hexafluoroarsenate (Ozark-Mahoning) were used as received. 1,2-bis(diphenylphosphino)ethane (Pressure Chemical) was recrystallized from absolute ethanol and dried in vacuo. Tetra-*n*-butylammonium perchlorate (TBAP, Pfaltz and Bauer) was recrystallized thrice from a mixture of hexane and ethyl acetate, dried in vacuo at 140 °C, and stored in a desiccator over P_2O_5. Tetrahydrofuran (Fisher) was stirred with $LiAlH_4$ for 24 h, fractionally distilled under an argon atmosphere, and stored in a Schlenk flask equipped with a Teflon stopcock. Acetonitrile (Fisher) was stirred over $KMnO_4$ for 24 h at room temperature and refluxed until the formation of MnO_2 was complete. Decantation was followed by treatment with P_2O_5 and a small amount of diethylenetriamine, and the mixture was refluxed for 5 h followed by fractionation under an argon atmosphere. Calcium hydride (Aldrich) was added to the distillate and the mixture refractionated under an argon atmosphere.

Sodium pentacarbonylmanganate, $Na^+Mn(CO)_5^-$, was prepared from 0.5 g (1.28 mmol) of $Mn_2(CO)_{10}$ dissolved in 25 mL of THF. To this solution was added 2 mL of 0.1% (w/w) sodium amalgam, and the solution was stirred vigorously for 1 h.[52] The complete formation of $NaMn(CO)_5$ was indicated by IR analysis (ν_{CO} = 1865 and 1900 cm^{-1}). After removal of the excess amalgam, the yellow solution was passed through Celite (Aldrich) and a solution consisting of 1 g (2.56 mmol) of tetraphenylphosphonium chloride in 10 mL of dichloromethane added. After removal of NaCl, hexane was added to precipitate $Ph_4P^+Mn(CO)_5^-$. **Tetraphenylarsonium tetracarbonyl(triphenylphosphine)manganate**, $Ph_4As^+Mn(CO)_5PPh_3^-$, was prepared by an analogous reduction of $Mn_2(CO)_8(PPh_3)_2$ with 1% sodium amalgam followed by precipitation of the arsonium salt by the procedure of Wrighton and Faltynek.[53] **Tetra-*n*-butylammonium tricarbonylbis(triphenylphosphine)manganate**, n-$Bu_4N^+Mn(CO)_3(PPh_3)_2^-$, was prepared in situ by the cathodic reduction of $(CO)_3(PPh_3)_2MnBr$ in THF solution containing 0.5 M TBAP.[13b] Tetra-*n*-butylammonium dicarbonylbis(bis(diphenylphosphino)ethane)-manganate, n-$Bu_4N^+(CO)_2(DPPE)_2Mn^-$, was prepared in situ as described previously.[29] Hexacarbonylmanganese(I) tetrafluoroborate, $Mn(CO)_6^+BF_4^-$, was prepared by the procedure described by Beach and Gray.[54] The preparations of the other salts of the carbonylmanganese cations listed in Table IV were described previously.[55-59]

***cis*-Dicarbonylbis(bis(diphenylphosphino)ethane)manganese(I) hexafluoroarsenate**, $Mn(CO)_2(DPPE)_2^+AsF_6^-$, was prepared by the treatment of a solution of 1.13 g (1.25 mmol) of $HMn(CO)_2(DPPE)_2$[35] in 50 mL of dichloromethane by the portionwise addition of 0.65 g (1.5 mmol) of $Ph_3C^+AsF_6^-$ at 0 °C under an argon atmosphere. When the mixture was stirred for 1 h, the IR bands of $HMn(CO)_2(DPPE)_2$ at ν_{CO} = 1856 and 1965 cm^{-1} disappeared completely with the attendant growth of the carbonyl bands of I at ν_{CO} = 1894 and 1953 cm^{-1}. The volume of the solution was reduced to 10 mL in vacuo, and the residual solution was rapidly chromatographed at 0 °C on alumina (Aldrich, activity I) with an acetonitrile–diethyl ether mixture (90/10, v/v) as the eluant. Collection of the yellow band was followed by immediate precipitation with excess diethyl ether to afford 0.75 g (55%) of pure *cis*-$Mn(CO)_2(DPPE)_2^+AsF_6^-$. The molecular structure of *cis*-$Mn(CO)_2(DPPE)_2^+AsF_6^-$ shown in Figure 5 was established by X-ray crystallography of a single crystal of *cis*-$Mn(CO)_2(DPPE)_2^+AsF_6^-$ prepared by vapor diffusion of diethyl ether into a concentrated solution at 3 °C.[35]

Instrumentation. Infrared spectra were recorded on a Nicolet 10DX FT spectrometer with 0.1-mm NaCl cells. ^1H and ^{31}P NMR spectra were obtained on a JEOL FX90Q or Nicolet NT300-WB spectrometer, with chemical shifts reported relative to TMS and H_3PO_4, respectively. ESR spectra were recorded on a Varian E110 spectrometer with a DPPH lock. Air-sensitive manipulations were carried out in a Vacuum Atmospheres MO-41 inert-atmosphere box. The conventional cyclic voltammetry at $v < 100$ V s^{-1} as well as the preparative-scale electrolysis were previously described.[12b,13b] The microvoltammetric measurements were made with platinum microelectrodes (5-μm radius) connected to a locally constructed fast-scan potentiostat employing fast-response operational amplifiers (Motorola LF-357) that were driven by a Exact Model 628 function generator.[60] Data storage and manipulation were carried out with a Gould Biomation 4500 digital oscilloscope (9-ns time resolution) interfaced to a Compaq Deskpro Model 3 microcomputer and Hewlett-Packard 7470A plotter. The charging current was largely removed from the cyclic voltammograms by digital subtraction of the background currents. All fast-scan cyclic voltammograms were carried out in a grounded Faraday cage to minimize 60-Hz interference.

Cyclic Voltammetry of Carbonylmanganate Anions. In an inert-atmosphere box, $Ph_4P^+Mn(CO)_5^-$ (0.032 g, 6×10^{-5} mol) was charged into the working electrode compartment of a CV cell of airless design.[12b] To this solution was added 6 mL of a 0.1 M solution of $TBA^+PF_6^-$ in acetonitrile to yield a 1×10^{-2} M solution of $Mn(CO)_5^-$. The reference arm of the cell was filled and the platinum macroelectrode inserted. The cell was sealed and then removed from the glovebox. After insertion of the calomel reference electrode, the cyclic voltammetry at conventional scan rates (0.1–100 V s^{-1}) was performed. At these scan rates the oxidation wave of $Mn(CO)_5^-$ at $E_a = -0.12$ V (0.5 V s^{-1}) remained irreversible. The fast-scan cyclic voltammetry was performed by replacing the macroelectrode with a platinum microelectrode, using the same solution and cell. The other carbonylmanganates listed in Table II were treated in a similar manner. The dashed curve in Figure 2c represents the computer simulation[39] of the cyclic voltammogram based on planar diffusion for the experimental value of $E° = 0.08$ V and $\alpha = 0.5$ at $v = 175\,000$ V s^{-1}.

Preparative-Scale Electrooxidation of Carbonylmanganates. To the working electrode compartment of a three-compartment bulk electrolysis cell was charged $PPh_4^+Mn(CO)_5^-$ (0.083 g, 1.55×10^{-4} mol), and 31 mL of acetonitrile containing 0.1 M $TBA^+PF_6^-$ was added. Four milliliters of the solvent–electrolyte solution was added to the reference arm as well as 6 mL to the counter electrode compartment, and the cell was sealed. When a constant-potential electrolysis was performed at +0.5 V vs SCE, it resulted in the uptake of 14.8 C corresponding to 0.99 electron/mol of $Mn(CO)_5^-$ charged. The IR spectrum of the solution after electrolysis indicated the presence of $Mn_2(CO)_{10}$ as the only carbonyl-containing product. The bulk electrolysis cell described above was alternatively charged with $AsPh_4^+Mn(CO)_4PPh_3^-$ (0.125 g, 1.55×10^{-4} mol) and 31 mL of acetonitrile containing 0.1 M $TBA^+PF_6^-$. The constant-potential electrolysis of this solution at 0.0 V resulted in the uptake of 15.1 C of

(50) The relative insensitivity of the CV simulation to values of k_d in the range of 0–100 M^{-1} s^{-1} is due to its limited competition with the very rapid first-order rate process, k_f in eq 24.
(51) Marcus, R. A. *J. Chem. Phys.* **1956**, *24*, 966. Marcus, R. A. *J. Chem. Phys.* **1957**, *26*, 867. Marcus, R. A. *J. Chem. Phys.* **1965**, *43*, 679.
(52) King, R. B.; Stone, F. G. A. *Inorg. Synth.* **1963**, *3*, 198.
(53) Wrighton, M. S.; Faltynek, R. A. *J. Am. Chem. Soc.* **1978**, *100*, 2701.
(54) Beach, N. W.; Gray, H. B. *J. Am. Chem. Soc.* **1968**, *90*, 5713.
(55) Darensbourg, M. Y.; Darensbourg, D. J. *Inorg. Chem.* **1975**, *14*, 1779.
(56) (a) Osborne, A. G.; Stiddard, M. H. B. *J. Chem. Soc.* **1965**, 700. (b) Sacco, A. *Gazz. Chim. Ital.* **1963**, *93*, 698.
(57) Treichel, P. M.; Mueh, H. J.; Bursten, B. E. *Isr. J. Chem.* **1976/77**, *15*, 253.
(58) (a) Treichel, P. M.; Firsich, D. W.; Essenmacher, G. J. *Inorg. Chem.* **1979**, *18*, 2405. (b) Treichel, P. M.; Mueh, H. J. *Inorg. Chem.* **1977**, *16*, 1167.
(59) Uson, R.; Riera, V.; Gimeno, J.; Laguna, M.; Gamasa, M. P. *J. Chem. Soc., Dalton Trans.* **1979**, 996.
(60) Howell, J. O.; Kuhr, W. G.; Ensman, R. E.; Wightman, R. M. *J. Electroanal. Chem. Interfacial Electrochem.* **1986**, *209*, 77.

charge corresponding to 1.01 electrons/mol of anion charged. The IR spectrum of the anolyte revealed $Mn_2(CO)_8(PPh_3)_2$[61] as the only carbonyl-containing product. Quantitative IR analysis from an absorbance vs concentration plot of an authentic sample of $Mn_2(CO)_8(PPh_3)_2$ indicated a yield of 92% based on $Mn(CO)_4PPh_3^-$ charged. When a 5×10^{-3} M solution of $NBu_4^+Mn(CO)_3(PPh_3)_2^-$ was oxidized at a constant potential of −0.5 V vs SCE, 15.0 C of charge was consumed, which corresponded to 1.00 electrons/mol of $Mn(CO)_3(PPh_3)_2^-$ charged. The IR spectrum of the anolyte revealed the quantitative formation of $HMn(CO)_3(PPh_3)_2$.[13b] For the electroxidation of $Mn(CO)_2(DPPE)_2^-$, the initial positive-scan cyclic voltammogram at $v = 500$ mV s^{-1} in THF showed a reversible anodic wave at $E_a = 1.39$ V (Figure 6) and an irreversible anodic wave at −0.45 V. Accordingly, a freshly reduced solution of 5 mM *cis*-$Mn(CO)_2(DPPE)_2^+AsF_6^-$ in acetonitrile containing 0.1 M TBAP (prepared at 0 °C as described above) was oxidized at a constant potential of 0.0 V until the current fell to zero. An accurate coulometric value was not obtained owing to the uncertainty of the initial concentration of $Mn(CO)_2(DPPE)_2^-$, as described above. If we assumed a 70% yield of II, based on the amount of I charged, an electron uptake of ~1.3e was observed. IR analysis of the now yellow anolyte revealed carbonyl bands at 1909 (shoulder) and 1844 cm^{-1} corresponding to $HMn(CO)_2(DPPE)_2$, together with a pair of characteristic carbonyl bands at 1954 and 1895 cm^{-1} for I. The presence of a small amount of the isomeric *trans*-$Mn(CO)_2(DPPE)_2^+$ was indicated from the band at 1895 cm^{-1} being ~1.3 times the intensity of its 1954-cm^{-1} counterpart.[62] A broad, less intense carbonyl band at 2028 cm^{-1} was apparent, but it was not identified. The anolyte was transferred with the aid of a cannula into a round-bottom flask, and $Ph_3C^+AsF_6^-$ was added at 0 °C. The infrared spectrum of this solution showed that the shoulder at 1909 cm^{-1} and the peak at 1844 cm^{-1} had disappeared, with an increase in intensity of the bands at 1954 and 1895 cm^{-1} to indicate the formation of more I. Since the band at 1895 cm^{-1} was still 1.3 times as intense as the band at 1954 cm^{-1}, we concluded that ~15% of *trans*-$Mn(CO)_2(DPPE)_2^+$ was present.

Electroreduction of Carbonylmanganese(I) Cations. The conventional cyclic voltammetry of the various carbonylmanganese(I) cations listed in Table IV were carried out as described previously.[12b] The microvoltammetric measurements of these cations were performed as described above for the carbonylmanganates.

Cyclic Voltammetry of *cis*-$Mn(CO)_2(DPPE)_2^+$. In a typical procedure, a thoroughly dried CV cell and a stock solution of 0.3 M TBAP in THF contained in a Schlenk flask were taken into an inert-atmosphere box. A pipet with a glass-wool plug was filled with neutral alumina (Woelm, super 1) previously activated at 450 °C in vacuo (1 Torr) for 12 h. Six milliliters of the THF–TBAP solution was passed through the column into the working electrode compartment of the cell, and the solution was stirred. Removal of the THF–TBAP from the working electrode compartment of the cell with the aid of a hypodermic syringe was followed by a second passage over the activated alumina column into the working compartment of the CV cell. This process was repeated five times to ensure the removal of water and other trace impurities from the electrolyte as well as from the glass walls of the CV cell. This treatment resulted in very flat zero-current base lines in the CV traces. After this purification process, 4 mL of the THF–(0.3 M) TBAP solution was placed in the reference arm of the CV cell (separated from the working compartment via an ultrafine-porosity glass frit) and the cell sealed and removed from the glovebox. Under a flow of argon, 0.033 g (3.0×10^{-5} mol) of *cis*-$Mn(CO)_2(DPPE)_2^+AsF_6^-$ was added to the working electrode compartment of the cell, and the Pt working electrode was inserted. Both the negative- and positive-scan cyclic voltammograms were then collected at a variety of sweep rates. Electrode pollution was evident after approximately four to five scans (reductions only) by the severe peak broadening and the decreased current heights. Removing the working electrode and polishing with 0.1-μm alumina powder followed by polishing on soft velvet and reinserting the electrode completely restored the original integrity of the CV traces. An identical procedure was carried out when acetonitrile solvent was used. In this case, only 0.1 M TBAP was used and electrode pollution was also evident and was rectified as described above. The fast-scan electrochemistry was carried out in the more polar acetonitrile and was performed by simply replacing the platinum macroelectrode with a microelectrode (Pt, 5-μm radius). Polishing of the microelectrode was required after every scan. Peak potentials and currents were calibrated relative to those of a ferrocene standard ($E^\circ = +0.534$ V vs SCE in (0.3 M) TBAP–THF and $E^\circ = +0.406$ V in (0.1 M) TBAP–CH_3CN). All voltages were referenced to the saturated calomel reference electrode with the connection made via an aqueous, saturated KCl salt bridge.

Preparative-Scale Electroreduction of *cis*-$Mn(CO)_2(DPPE)_2^+$. A thoroughly dried three-compartment electrolysis cell was removed from a 150 °C oven and allowed to cool in vacuo. In a separate, thoroughly dried, round-bottom flask equipped with a sidearm, a 50-mL stock solution of 0.1 M TBAP–CH_3CN was prepared. The cell was charged with 31 mL of the electrolyte solution to the working electrode compartment, 10 mL to the counter electrode compartment, and 5 mL to the reference arm under an argon atmosphere. The reference electrode and counter electrode (doubly coiled nichrome wire embedded in a 14/20 standard taper joint) were inserted, and the cell was sealed. Prereduction of the acetonitrile was carried out at a constant potential of −2.2 V until the current fell to zero. The cell was then chilled to 0 °C, and 0.33 g (3×10^{-4} mol) of *cis*-$Mn(CO)_2(DPPE)_2^+AsF_6^-$ was added under a flow of argon to afford a 1.0×10^{-2} M solution. The controlled-potential reduction of the light yellow-green solution at −2.0 V was carried out until the current fell to the background level; at this point a very dark red solution resulted. Coulometry indicated the passage of 56.3 C, which corresponded to 1.94 equiv of charge/mol of $Mn(CO)_2(DPPE)_2^+$ added. IR analysis of the dark red catholyte revealed four bands in the carbonyl region, namely a pair at 1710 and 1766 cm^{-1} for $Mn(CO)_2(DPPE)_2^-$ and a pair at 1909 and 1844 cm^{-1} for $HMn(CO)_2(DPPE)_2$.[63] The yield of II was approximately 70% based on IR intensity of the carbonyl bands. CV analysis revealed the complete absence of the cathodic wave of I and the presence of an anodic wave with a reversible couple at −1.44 V and an irreversible anodic wave at −0.67 V. When the same electrolysis is carried out in THF–(0.3 M) TBAP and 5×10^{-3} M *cis*-$Mn(CO)_2(DPPE)_2^+$, 1.95 equiv of charge was taken up at a constant potential of −2.0 V. The dark red solution upon IR analysis revealed only a 40% yield of II, with the remainder consisting of $HMn(CO)_2(DPPE)_2$. CV analysis revealed the reversible II/17e couple at $E^\circ = -1.45$ V and the irreversible oxidation of 17e at −0.45 V (vide supra). These results completely mimicked those of the preparative-scale electrolytic reduction of the trans isomer, both in the coulometry observed and in the ratio of products (anion to hydride) obtained.[29] However, for the product analysis, acetonitrile was the preferred solvent since II was more persistent in this medium.

Digital Simulation of the Cyclic Voltammograms. The computer simulations were carried out by the finite difference method of Feldberg.[38,39] The simulation of a full-cycle cyclic voltammogram consisted of 1000 discrete data points to allow for good resolution when the simulated cyclic voltammograms were compared with the experimental voltammograms. The following rate processes and equations were employed:

$$19e \underset{k_b}{\overset{k_f}{\rightleftharpoons}} 17e$$

$$I + II \underset{k_d}{\overset{k_{et}}{\rightleftharpoons}} 19e + 17e$$

$$d[19e]/dt = k_{et}[I^+][II^-] + k_b[17e]$$

$$d[17e]/dt = k_f[cis\text{-}19e] + k_{et}[I^+][II^-]$$

The heterogeneous rate constant $k_s = 4.0 \times 10^{-3}$ cm s^{-1} for wave A and the standard reduction potential $E_1^\circ = -1.61$ V were set to yield $E_c = -1.71$ V with the experimentally determined transfer coefficient $\alpha = 0.40$.[64] The parameters for the II/17e couple were the experimental values $k_s = 1.1 \times 10^{-2}$ cm s^{-1}, $E_2^\circ = -1.45$ V, and $\alpha = 0.45$. The diffusion coefficients of all species were set equal to the experimentally determined value of $D = 6 \times 10^{-6}$ cm^2 s^{-1} for II.[10a] Inclusion of the rates of disappearance and the heterogeneous electron-transfer kinetics, as described earlier, defines the concentration of all species at any given distance from the electrode.[35,42]

CV Determination of the Dimerization Rate Constant. For the EC_{dim} mechanism in Scheme I, the theoretically defined current ratio is given by Nicholson et al.[27] as a function of ω, where $\log \omega = \log (k_2 C_0^* t) + 0.034(at - 4)$ with $at = n\mathcal{F}/RT(E_t - E^\circ)$. E_t is the switching potential, and t is the time from E_t to E° (or $E_{1/2}$). For $Mn(CO)_4PPh_3^-$, the experimentally determined current ratios i_c/i_a (at v and t) are as follows: 0.5 (1000 V s^{-1}, 2.6×10^{-4} s); 0.65 (2000 V s^{-1}, 1.3×10^{-4} s); 0.97 (4000 V s^{-1}, 6.5×10^{-5} s^{-1}); 1.0 (6000 V s^{-1}, 4.33×10^{-5} s). These values yield $\omega = 4.48$, 1.44, 0.06, and 0.02, respectively, from the aforementioned working curve of the theoretical current ratio versus ω.[27] A plot of ω vs t resulted in a straight line with correlation coefficient 0.995 in which the slope was $2.13 \times 10^5 = k_2 C_0^* \exp[0.078(at - 4)]$, where $C_0^* = 1.0 \times 10^{-2}$ M, $E_t = -0.140$ V, and $E^\circ = -0.40$ V. The derived value of $k_2 = 1.4$

(61) See Darensbourg in ref 55.
(62) For a discussion of this analysis, see ref 35.
(63) A similar situation occurs in the reduction of the isomeric *trans*-$Mn(CO)_2(DPPE)_2^+$, and the accompanying formation of the hydride $HMn(CO)_2(DPPE)_2$ from II is detailed in ref 29.
(64) Nadjo, L.; Saveant, J. M. *J. Electroanal. Chem. Interfacial Electrochem.* **1973**, *48*, 113.

$\times 10^7$ M^{-1} s^{-1} compared with 1×10^7 M^{-1} s^{-1} evaluated by Brown and co-workers.[22]

The application of the same procedure to $Mn(CO)_5^-$ failed to produce reproducible results owing to the large corrections for the charging current and ohmic drop at the requisite fast scan rates in Table I. An approximate value of k_2 was obtained from the relationship $k_2 = n\mathcal{F}v/(C_0^*RT)$ when $i_c/i_a \cong 1$, as also derived by Nicholson and co-workers.[27] For $Mn(CO)_5^-$, this current ratio was attained at $v \simeq 175\,000$, from which $k_2 = 7 \times 10^8$ M^{-1} s^{-1}, in reasonable agreement with a value of $k_2 = 9 \times 10^8$ M^{-1} s^{-1} evaluated by Brown and co-workers.[22] The validity of this relationship is supported by the value of $k_2 = 1.5 \times 10^7$ M^{-1} s^{-1} for $Mn(CO)_4PPh_3^-$ obtained at $v = 4000$ for $i_c/i_a = 1.0$ (vide supra).

Acknowledgment. We thank the National Science Foundation and the R. A. Welch Foundation for financial support.

Registry No. I, 47902-58-9; I·AsF_6^-, 117872-92-1; II, 115162-69-1; $Mn(CO)_5^-$, 14971-26-7; $Mn(CO)_4PPh_3^-$, 53418-18-1; $Mn(CO)_2(\eta^2\text{-DPPE})_2^\bullet$, 118490-97-4; $Mn(CO)_2(\eta^2\text{-DPPE})(\eta^1\text{-DPPE})^\bullet$, 115162-72-6; $Mn(CO)_3(Ph_3P)_2^-$, 68033-53-4; $Mn(CO_3)(DPPE)^-$, 113821-86-6; $Mn(CO_3)((PhO)_3P)_2^-$, 68033-46-5; $Mn(CO_3)((o\text{-}CH_3C_6H_4O)_3P)_2^-$, 84180-09-6; $Mn(CO_3)((n\text{-}Bu_3)P)_2^-$, 113821-87-7; $Mn(CO_3)((i\text{-}PrO)_3P)_2^-$, 113890-85-0; $Mn(CO_3)((i\text{-}Pr)_3P)_2^-$, 113821-88-8; $Mn(CO_6)^+BF_4^-$, 15557-71-8; $Mn(CO)_5PPh_3^+BF_4^-$, 54039-46-2; $Mn(CO)_3(NCCH_3)_3^+BF_4^-$, 68928-06-3; *trans*-$Mn(CO)_2(DPPE)_2^+PF_6^-$, 34216-61-0; *cis*-$Mn(CO)_2(CNCH_3)_4^+PF_6^-$, 65546-42-1; $Mn(CNC_6H_4CH_3)_6^+PF_6^-$, 118419-41-3; *cis*-$Mn(CO)_2[P(OMe)_3]_4^+BF_4^-$, 118419-39-9; $Mn(CO)_5^\bullet$, 14971-26-7; $Mn(CO)_3(PPh_3)_2^\bullet$, 27903-25-9; $Mn(CO)_4PPh_3^\bullet$, 14971-47-2; $Mn(CO)_3[P(OPh)_3]_2^\bullet$, 113821-89-9; *trans*-$Mn(CO)_2(DPPE)_2^+$, 47902-56-7; Pt, 7440-06-4; carbon monoxide, 630-08-0; tetra-*n*-butylammonium hexafluorophosphate, 3109-63-5.

Contribution from the Department of Chemistry, University of Tennessee, Knoxville, Tennessee 37996, and Savannah River Laboratory, E. I. du Pont de Nemours & Company, Inc., Aiken, South Carolina 29808

Electrocatalytic Reduction of Nitrate in Sodium Hydroxide Solution in the Presence of Low-Valent Cobalt-Cyclam Species

Hu-Lin Li,[†,‡] William C. Anderson,[†] James Q. Chambers,*[,†] and David T. Hobbs[§]

Received August 26, 1988

In concentrated NaOH solution nitrate and nitrite ions are efficiently reduced to a mixture of products including hydroxylamine and ammonia via an electrocatalytic process in the presence of cobalt complexes of 1,4,8,11-tetraazacyclotetradecane (cyclam). A key mechanistic role is proposed for Co^I(cyclam)NO_3, which is generated in the diffusion layer at ca. −1.3 V vs SCE. The lack of dependence on pH of either the catalytic peak potential or the peak current indicates that metal hydride intermediate species are not involved in the initial steps of the reduction process. Both Co^I and Co^{III} intermediates in the nitrate reduction are detected in collection experiments with a gold ring–disk electrode.

Transition-metal macrocyclic amine complexes based on ligands such as 1,4,8,11-tetraazacyclotetradecane have the property of catalyzing a variety of redox processes of a remarkable diversity.[1-6] Electrocatalytic reductions of dioxygen,[3] carbon dioxide,[1,2,4] the N–O bond in nitrate and nitrite,[6] and carbon–halogen bonds[5] have been reported. Schemes suggested to explain the electrocatalytic activity of the these species generally invoke the chemical stability imparted to the lower oxidation states by the macrocylic ligand and the chemistry made possible by the availability of the labile axial coordination sites.

Of particular interest to us were the reports by Taniguchi et al.[6] that metal cyclam complexes, specifically the classical 14-membered 1,4,8,11-tetraazacyclotetradecane macrocycle complexes of cobalt and nickel, act as excellent catalysts for the reduction of nitrate and nitrite in aqueous solutions. As part of a project involving the destruction of nitrate in nuclear waste solutions, the reduction of nitrate and nitrite in concentrated sodium hydroxide solutions has been under study in our laboratories for some time.[7,8] At several metal and phthalocyanine-coated electrodes nitrate and nitrite ions are reduced to mixtures of products that include dinitrogen, hydroxylamine, and ammonia. These electrode reactions, which are not diffusion-limited, give rise to voltammetric currents that increase exponentially at the foot of the hydrogen discharge process. The present study was undertaken to determine the compatibility of the metal–cyclam electrocatalyzed cycle for the reduction of nitrate under the strongly alkaline conditions that are encountered in the treatment of nuclear waste solutions. Several details regarding the role of reduced Co(cyclam) species in the mechanism of the nitrate reduction have been revealed in the course of the study.

Experimental Section

Chemicals. Reagent grade chemicals and doubly distilled water that had been passed through a Millipore purification column were used to prepare all solutions. The [*trans*-Cl_2Co^{III}(cyclam)]Cl complex, where cyclam is 1,4,8,11-tetraazacyclotetradecane (Aldrich), was prepared by literature procedures.[9] Ferrozine, 3-(2-pyridyl)-5,6-diphenyl-1,2,4-triazine-4,4′-disulfonic acid, was obtained from Fluka. The deuterated reagents NaOD and D_2O were obtained from the Cambridge Isotope Laboratory.

Electrodes and Cells. The working electrodes for voltammetry were disk electrodes constructed from lead rod (Aldrich, 99.9995%), gold wire (Aldrich, 99.99%), silver wire (GR), and a mercury surface prepared by electroplating a gold disk; the geometrical areas for the electrodes were 0.126, 0.0314, 0.002, and 0.0113 cm^2, respectively. Larger area electrodes were used for the controlled-potential electrolyses. A large area nickel plate was used for the counter electrode. A SCE was the reference electrode in all experiments. The rotating gold ring–gold disk electrode (Pine Instrument Co., Model AFDT27) had dimensions of $r_1 = 0.250$ cm, $r_2 = 0.2705$ cm, and $r_3 = 0.3325$ cm.

Simple glass cells with provision for oxygen removal by flushing with argon were employed. "High-purity" argon was purified further by passage through a 3-ft column containing Mn(II) dispersed on vermiculite.[10]

Instrumentation. Electrochemical experiments were carried out by using a Bioanalytical Systems electrochemical analyzer, Model BAS-100.

[†] University of Tennessee.
[‡] Present address: Department of Chemistry, Lanzhou University, Ganzu, China.
[§] E. I. du Pont de Nemours & Co., Inc.

(1) Fisher, B.; Eisenberg, R. *J. Am. Chem. Soc.* **1980**, *102*, 7361.
(2) Beley, M.; Collin, J.-P.; Ruppert, R.; Sauvage, J.-P. *J. Am. Chem. Soc.* **1986**, *108*, 7461.
(3) Geiger, T.; Anson, F. C. *J. Am. Chem. Soc.* **1981**, *103*, 7489.
(4) Bradley, M. G.; Tysak, T.; Graves, D. J.; Vlachopoulos, N. A. *J. Chem. Soc., Chem. Commun.* **1983**, 349.
(5) (a) Becker, J. Y.; Kerr, J. B.; Pletcher, D.; Rosas, R. *J. Electroanal. Chem. Interfacial Electrochem.* **1981**, *117*, 87. (b) Gosden, C.; Kerr, J. B.; Pletcher, D.; Rosas, R. *Ibid.* **1981**, *117*, 101.
(6) (a) Taniguchi, I.; Nakashima, N.; Yasukouchi, K. *J. Chem. Soc., Chem. Commun.* **1986**, 1814. (b) Taniguchi, I.; Nakashima, N.; Matsushita, K.; Yasukouchi, K. *J. Electroanal. Chem. Interfacial Electrochem.* **1987**, *224*, 199.
(7) Li, H.-L.; Robertson, D. H.; Chambers, J. Q.; Hobbs, D. T. *J. Electrochem. Soc.* **1988**, *135*, 1154.
(8) Li, H.-L.; Chambers, J. Q.; Hobbs, D. T. *J. Appl. Electrochem.* **1988**, *18*, 454.
(9) Bosnich, B.; Poon, C. K.; Tobe, M. L. *Inorg. Chem.* **1965**, *4*, 1102.
(10) Brown, T. L.; Dickerhoot, C. W.; Bafus, D. A.; Morgan, G. L. *Rev. Sci. Instrum.* **1962**, *22*, 491.

0020-1669/89/1328-0863$01.50/0